ELSEVIER

Journal of Chromatography A, 865 (1999) 13–25

JOURNAL OF CHROMATOGRAPHY A

www.elsevier.com/locate/chroma

Modeling and simulation of the dynamic behavior of monoliths Effects of pore structure from pore network model analysis and comparison with columns packed with porous spherical particles

A.I. Liapis*, J.J. Meyers, O.K. Crosser

Department of Chemical Engineering and Biochemical Processing Institute, University of Missouri-Rolla, Rolla, MO 65409-1230, USA

Abstract

A mathematical model is presented that could be used to describe the dynamic behavior, scale-up, and design of monoliths involving the adsorption of a solute of interest. The value of the pore diffusivity of the solute in the pores of the skeletons of the monolith is determined in an a priori manner by employing the pore network modeling theory of Meyers and Liapis [J. Chromatogr. A, 827 (1998) 197 and 852 (1999) 3]. The results clearly show that the pore diffusion coefficient, D_{mp}, of the solute depends on both the pore size distribution and the pore connectivity, n_T, of the pores in the skeletons. It is shown that, for a given type of monolith, the film mass transfer coefficient, K_f, of the solute in the monolith could be determined from experiments based on Eq. (3) which was derived by Liapis [Math. Modelling Sci. Comput., 1 (1993) 397] from the fundamental physics. The mathematical model presented in this work is numerically solved in order to study the dynamic behavior of the adsorption of bovine serum albumin (BSA) in a monolith having skeletons of radius $r_o=0.75\cdot10^{-6}$ m and through-pores having diameters of $1.5\cdot10^{-6}$–$1.8\cdot10^{-6}$ m [H. Minakuchi et al., J. Chromatogr. A, 762 (1997) 135]. The breakthrough curves of the BSA obtained from the monolith were steeper than those from columns packed with porous spherical particles whose radii ranged from $2.50\cdot10^{-6}$ m to $15.00\cdot10^{-6}$ m. Furthermore, and most importantly, the dynamic adsorptive capacity of the monolith was always greater than that of the packed beds for all values of the superficial fluid velocity, V_{tp}. The results of this work indicate that since in monoliths the size of through-pores could be controlled independently from the size of the skeletons, then if one could construct monolith structures having (a) relatively large through-pores with high through-pore connectivity that can provide high flow-rates at low pressure drops and (b) small-sized skeletons with mesopores having an appropriate pore size distribution (mesopores having diameters that are relatively large when compared with the diameter of the diffusing solute) and high pore connectivity, n_T, the following positive results, which are necessary for obtaining efficient separations, could be realized: (i) the value of the pore diffusion coefficient, D_{mp}, of the solute would be large, (ii) the diffusion path length in the skeletons would be short, (iii) the diffusion velocity, v_D, would be high, and (iv) the diffusional response time, t_{drt}, would be small. Monoliths with such pore structures could provide more efficient separations with respect to (a) dynamic adsorptive capacity and (b) required pressure drop for a given flow-rate, than columns packed with porous particles.

Keywords: Monolithic columns; Computer simulation; Mathematical modeling; Continuous beds; Network model; Mass transfer; Pore diffusion; Pore size distribution; Pore connectivity; Albumins

*Corresponding author. Tel.: +1-573-3414-416; fax: +1-573-3412-071.

0021-9673/99/$ – see front matter
PII: S0021-9673(99)01031-6

1. Introduction

The problem of a high column pressure drop associated with a column packed with small particles could be overcome through the use of a column made of one piece of a porous solid (continuous porous column or monolith) [1–16]. Minakuchi et al. [14] have constructed porous silica rods (monoliths) that possess a biporous structure consisting of through-pores and mesopores. The through-pores provide the channels for bulk convective flow while the mesopores are located in the silica skeletons and the surface of the mesopores provides the internal surface area of the monolith on which adsorption of adsorbate molecules occurs. The size of the through-pores can be varied independently from the size of the skeletons [14] in the monolith, and Minakuchi et al. [14] have shown experimentally that silica monoliths having skeletons of 1–1.7 μm and through-pores of 1.5–1.8 μm in diameter, could provide higher column efficiency at high linear velocities and a smaller pressure drop than columns packed with porous silica particles having a diameter of 5 μm. Meyers and Liapis [15,16] have constructed and solved a pore network model that together with the experimental information obtained from (i) scanning electron microscopy (SEM), (ii) transmission electron microscopy (TEM), (iii) mercury intrusion porosimetry, (iv) size-exclusion chromatography (SEC) and (v) adsorption capacity experiments, could determine in an a priori manner the pressure drop and the values of the parameters that characterize the mass transfer mechanisms of convective flow and diffusion of molecules adsorbing in monoliths and in columns packed with porous purely diffusive or perfusive adsorbent particles [15–25].

In this work, a model for monoliths possessing a biporous structure is constructed and employed to study the dynamic adsorptive capacity of a monolith as the linear velocity of the fluid in the through-pores is varied. The results are compared with those obtained in columns packed with spherical porous adsorbent particles.

2. Model formulation

Single-component adsorption is considered to take place in a monolith possessing a biporous structure of through-pores and mesopores, and consisting of skeletons whose shape could be approximated by cylindrical or spherical geometry [14]. A differential mass balance for the adsorbate in the fluid stream flowing in the through-pores of the monolith gives

$$\epsilon_{tp}\cdot\frac{\partial C_{tp}}{\partial t}+V_{tp}\cdot\frac{\partial C_{tp}}{\partial x}-\epsilon_{tp}D_{tp}\cdot\frac{\partial^2 C_{tp}}{\partial x^2}=$$
$$(1-\epsilon_{tp})\left(\frac{\alpha+1}{r_o}\right)\cdot K_f\left[C_{mp}(t,x,r_o)-C_{tp}\right] \qquad (1)$$

In Eq. (1) the superficial fluid velocity in the through-pores, V_{tp}, is taken to be independent of the space variable, x, because the liquid solution is considered to be dilute and the main component of the solution is the carrier fluid (for non-dilute solutions, a material balance, as shown in Ref. [26], would provide the expression for $\partial V_{tp}/\partial x$). The pressure drop through the monolith could be determined by the pore network modeling theory developed by Meyers and Liapis [15,16].

The film mass transfer coefficient, K_f, in Eq. (1) could be determined from the expression derived by Liapis [18] which is given by the following equation:

$$\frac{K_f\lambda}{D_{mf}}=\mathrm{Sh}=\alpha_1\mathrm{Pe}^{1/3} \qquad (2)$$

Eq. (2) was derived for a through-pore of arbitrary geometry and indicates that the Sherwood number (Sh) is proportional to $\mathrm{Pe}^{1/3}$; Pe is the Peclet number ($\mathrm{Pe}=v_m\lambda/D_{mf}$), λ denotes the linear characteristic dimension of a through-pore in the monolith, and α_1 is the proportionality constant. It should be noted here that for through-pores of cylindrical geometry, as well as for boundary layers around particles of spherical geometry [27,28], it has been shown that $K_f\lambda/D_{mf}$ is proportional to $\mathrm{Pe}^{1/3}$. But Liapis [18] has shown that the Sherwood number, $K_f\lambda/D_{mf}$, is proportional to $\mathrm{Pe}^{1/3}$ (Eq. (2)) for a through-pore of arbitrary geometry. Furthermore, Liapis [18] has shown that

$$K_f\propto(D_{mf})^{2/3}\left(\frac{1}{\mu}\right)^{1/3}\left(\frac{\Delta P}{L}\right)^{1/3} \qquad (3)$$

The result shown in Eq. (3) indicates that the film mass transfer coefficient, K_f, is independent of λ. This implies that in a monolith or in a fixed bed of

particles with through-pores having similar geometry but different sizes, the film mass transfer coefficient, K_f, would be the same for all through-pores and would have a constant value for a given $\Delta P/L$ and temperature. Because from Eq. (3) K_f is proportional to $(\Delta P/L)^{1/3}$, and since $\Delta P/L$ for a monolith has been found [14] to be less than $\Delta P/L$ for a packed bed of spherical particles at the same superficial velocity, V_{tp}, then the value of K_f for the monolith could be smaller than the value of K_f in a packed bed of spherical particles. Eq. (1) could be used for monoliths whose skeletons have geometry of cylinders or spheres by putting $\alpha=1$ or 2, respectively. The initial and boundary conditions of Eq. (1) are as follows:

$$C_{tp} = 0 \quad \text{at } t = 0, \quad 0 \le x \le L \tag{4}$$

$$\frac{V_{tp}}{\epsilon_{tp}} C_{tp} - D_{tp} \frac{\partial C_{tp}}{\partial x} = \frac{V_{tp}}{\epsilon_{tp}} C_{tp,in} \quad \text{at } x = 0, t > 0 \tag{5}$$

$$\frac{\partial C_{tp}}{\partial x} = 0 \quad \text{at } x = L, t > 0 \tag{6}$$

In certain monoliths [14] the axial dispersion coefficient, D_{tp}, could be so low that by setting its value equal to zero, the error introduced in the prediction of the behavior of an adsorption system might not be significant. When D_{tp} is set equal to zero, the term D_{tp} $(\partial^2 C_{tp}/\partial x^2)$, in Eq. (1), becomes equal to zero, and the boundary condition at $x=0$ (Eq. (5)) becomes as follows:

$$C_{tp} = C_{tp,in} \quad \text{at } x = 0, t > 0 \tag{7}$$

The transport of the adsorbate in the skeletons is considered to be governed by the diffusion [17,29–33] of the adsorbate molecules in the pore fluid (pore diffusion) of the skeletons. The intraparticle pore diffusion mechanism is taken to be one dimensional and in skeletons that have an axis of symmetry. A differential material balance for the adsorbate in the skeleton is given by

$$\frac{\partial(\epsilon_{mp} C_{mp})}{\partial t} + \frac{\partial C_{smp}}{\partial t} = \frac{1}{r^{\alpha}} \cdot \frac{\partial}{\partial r}\left(r^{\alpha} \epsilon_{mp} D_{mp} \cdot \frac{\partial C_{mp}}{\partial r} \right) \tag{8}$$

The initial and boundary conditions for Eq. (8) are

$$C_{mp} = 0 \quad \text{at } t = 0, \quad 0 \le r \le r_o, \quad 0 \le x \le L \tag{9}$$

$$C_{smp} = 0 \quad \text{at } t = 0, \quad 0 \le r \le r_o, \quad 0 \le x \le L \tag{10}$$

$$-\epsilon_{mp} D_{mp} \left.\frac{\partial C_{mp}}{\partial r}\right|_{r=r_o} = K_f\left[C_{mp}(t, x, r_o) - C_{tp}\right], \quad t > 0 \tag{11}$$

$$\left.\frac{\partial C_{mp}}{\partial r}\right|_{r=0} = 0, \quad t > 0 \tag{12}$$

If restricted pore diffusion occurs [16,33–35], then ϵ_{mp} and D_{mp} would vary with the loading of the adsorbate in the adsorbed phase, as shown in Refs. [16,33,35]. If the effect of restricted pore diffusion on the mass flux of the adsorbate is not significant, then the values of ϵ_{mp} and D_{mp} in Eq. (8) may be considered to be constant [15,16,29–35]. The values of ϵ_{mp} and D_{mp} can be determined by the pore network modeling theory developed by Meyers and Liapis [15,16].

If in addition to pore diffusion there is convective flow in the pores of the skeletons, the values of the convective velocity and of the pore diffusion coefficient can be obtained from the expressions derived in the pore network modeling theory of Meyers and Liapis [15,16]. In this case, Eq. (8) has to be augmented in order to account for the contribution of convective flow in the pores of the skeletons as in the case of perfusion chromatography [15,16,18–25,36–42]. In this work, as stated above, monoliths possessing a biporous structure are considered and convective flow is taken to occur only in the through-pores of the monolith while the mesopores in the skeletons [14] have pore diameters of such size that only pore diffusion is considered to occur (e.g., silica rods [14]).

The term $\partial C_{smp}/\partial t$ in Eq. (8) represents the accumulation of the adsorbed species on the surface of the pores (mesopores [14]) in the skeletons, and it can be quantified by employing a mathematical expression that could describe the mechanism of the adsorption of the adsorbate onto the active sites immobilized on the surface of the pores in the skeletons. In this work, the rate of the adsorption step is considered to be described by the following second-order reversible mechanism:

$$\frac{\partial C_{smp}}{\partial t} = k_1 C_{mp}(C_{smp,max} - C_{smp}) - k_2 C_{smp} \qquad (13)$$

The initial condition of Eq. (13) is given by Eq. (10).

The simultaneous solution of the coupled Eqs. (1), (8) and (13) was obtained numerically. The method of orthogonal collocation [43,44] was applied to the space variables x and r of the partial differential Eqs. (1) and (8), and the resulting ordinary non-linear differential equations were numerically integrated by using Gear's method [44], which is employed in the LSODES component of the ODEPACK [45] software package.

3. Results and discussion

The functional form of the Gaussian distribution given by

$$f(d) = \left(\frac{1}{\sqrt{2\pi}\sigma}\right) \exp\left[-\frac{1}{2} \cdot \left(\frac{d-\gamma}{\sigma}\right)^2 \right] \qquad (14)$$

is taken to represent the pore size distribution (PSD) of the pores (mesopores) in the skeletons or in the particles. The pores in the skeletons or in the particles are topologically mapped onto a cubic lattice network of interconnected cylindrical pores [15,16] and the assignment of the pores (mesopores) in the network was taken, in this work, to be random. The cubic lattice has a regular array of nodes that are connected to each other by bonds (pores) of the network. A lattice size of $15\times15\times15$ was used, which, from previous experience with random networks [15,16,46,47], would be expected to provide a reasonably satisfactory representation of the pore network and does not require excessive computational times. The parameter d in Eq. (14) represents the pore diameter, γ denotes the mean diameter of the pores, and σ is the standard deviation of the diameter of the pores. Two different sets for the parameters γ and σ were considered in Eq. (14) resulting in the following two pore size distributions: (i) PSD I has $\gamma=240$ Å and $\sigma=120$ Å, and (ii) PSD II has $\gamma=240$ Å and $\sigma=60$ Å. A third pore size distribution was also considered in this work denoted by PSD III in which all pores were taken to have a diameter equal to 240 Å; in PSD III the mean diameter of the pores is equal to 240 Å and the standard deviation of the diameter of the pores is equal to zero. The porosity ϵ_{mp} of the skeletons or of the particles was taken to be equal to 0.60 [14] and bovine serum albumin (BSA) was considered [24] to be the solute diffusing in the pores (mesopores) of the skeletons or in the pores of the particles. The free molecular diffusivity, D_{mf}, of BSA is $5.9\cdot10^{-11}$ m^2/s at room temperature [24,48] and the diameter of the BSA molecule is about 65 Å. In Table 1 the values of the pore diffusivity, D_{mp}, of BSA in the pores of the skeletons or in the pores of the particles are presented for PSD I, PSD II, and PSD III, as well as for different values of the pore connectivity n_T. The pore connectivity, n_T, is defined as the number of pores (mesopores) connected to a single node of the lattice. The values of D_{mp} in Table 1 were determined from the pore network modeling theory developed by Meyers and Liapis [15,16]. Simulations of the model porous medium using the pore size distributions mentioned above yield a percolation threshold at pore connectivity of 2.76. Pore connectivities below this value do not produce a percolating cluster of mesopores, which is necessary for pore diffusion through the model porous medium. When n_T is equal to six, this means that the lattice network is completely occupied, since, in this case, the value of n_T is equal to the coordination number of the cubic lattice [15,16]. The results in Table 1 clearly show that, for a given pore size distribution, the value of the pore diffusion coefficient, D_{mp}, increases significantly as the pore connectivity, n_T, increases. Furthermore, the results in Table 1 indicate that the largest value of D_{mp} is obtained when the pore connectivity n_T is equal to six and the pore size distribution of the porous medium is represented by PSD III. The data in Table 1 strongly indicate that the value of the pore diffusion coefficient, D_{mp}, depends on both the pore size distribution and the pore connectivity n_T of the porous medium.

If one would consider the empirical relationship $D_{mp}=(\epsilon_{mp}D_{mf})(\delta/\tau)$, where δ represents the hindrance parameter of the porous medium [15,16,38,49] and τ denotes the average tortuosity in the porous medium, then the ratio $D_{mp}/(\epsilon_{mp}D_{mf})$ in Table 1 might be thought of as providing the value of the ratio δ/τ in an a priori manner. The results in

Table 1
Values of the pore diffusion coefficient, D_{mp}, of BSA in the pores of skeletons of monoliths or in the pores of particles packed in a column, for different values of the pore connectivity, n_T, and when the pore size distribution of the porous medium (porous skeleton or porous particle) is represented by the functional form of (i) PSD I, (ii) PSD II, and (iii) PSD III

Pore size distribution	n_T (dimensionless)	D_{mp} (m^2/s)	$D_{mp}/(\epsilon_{mp}D_{mf})=\delta/J$ (dimensionless)
PSD I	2.76	$0.647\cdot10^{-12}$	0.0183
PSD I	3.00	$0.813\cdot10^{-12}$	0.0230
PSD I	4.00	$1.753\cdot10^{-12}$	0.0495
PSD I	5.00	$2.733\cdot10^{-12}$	0.0772
PSD I	6.00	$3.612\cdot10^{-12}$	0.1020
PSD II	2.76	$0.769\cdot10^{-12}$	0.0217
PSD II	3.00	$1.191\cdot10^{-12}$	0.0336
PSD II	4.00	$2.328\cdot10^{-12}$	0.0658
PSD II	5.00	$3.598\cdot10^{-12}$	0.1016
PSD II	6.00	$4.728\cdot10^{-12}$	0.1336
PSD III	2.76	$1.522\cdot10^{-12}$	0.0430
PSD III	3.00	$1.890\cdot10^{-12}$	0.0534
PSD III	4.00	$3.686\cdot10^{-12}$	0.1041
PSD III	5.00	$5.864\cdot10^{-12}$	0.1656
PSD III	6.00	$7.760\cdot10^{-12}$	0.2192

Table 1 indicate that the pore network model [15,16] can be used to provide in an a priori manner numerical values for the pore diffusion coefficient, D_{mp}, which could then be employed in the dynamic macroscopic model of the monolith described by Eqs. (1)–(13) or in the macroscopic models that describe the dynamic behavior of chromatographic separations in columns packed with porous particles [17,29–32,50]. If the adsorption process of BSA leads to conditions of restricted pore diffusion [16,33–35] in a porous medium, then the value of D_{mp} would decrease with loading and could be determined in an a priori manner from the pore network modeling theory developed by Meyers and Liapis [16].

The diffusion velocity, v_D, of BSA in the pores of the skeletons or in the pores of the particles could be estimated (Carlson and Dranoff [51]) from the ratio D_{mp}/r_o where r_o is the radius of the skeleton or of the particle. Thus, as the value of the radius, r_o, decreases, the value of the diffusion velocity, v_D, increases. Another parameter of importance in systems involving intraparticle diffusion is the diffusional response time, t_{drt}, which could be estimated [51] from the ratio r_o^2/D_{mp}. Efficient separation systems would have low values of diffusional response time, and, for a given value of D_{mp}, the value of t_{drt} can be decreased when the value of the radius, r_o, is decreased. Since in monoliths the size of through-pores can be controlled independently from the size of skeletons [14], then if one could construct monolith structures having (a) relatively large through-pores with high through-pore connectivity that can provide high flow-rates at low pressure drops and (b) small-sized skeletons (skeletons having low values of r_o) with mesopores having an appropriate pore size distribution (mesopores having diameters that are relatively large when compared with the diameter of the diffusing solute) and high pore connectivity, n_T, the following positive results, which are necessary for obtaining efficient separations, could be realized: (i) the value of the pore diffusion coefficient, D_{mp}, would be large, (ii) the diffusion path length in the skeletons would be short, (iii) the diffusion velocity, v_D, would be high, and (iv) the diffusional response time, t_{drt}, would be small. Monoliths with such pore structures can provide more efficient separations with respect to (a) dynamic adsorptive capacity and (b) required pressure drop for a given flow-rate, than columns packed with porous particles. In packed beds, the size of the interstitial channels for bulk flow depends on the size

of the porous particles, and therefore, as the size, r_o, of the particles is reduced in order to decrease the diffusion path length in the particles, the size of the interstitial channels for bulk flow becomes very small and prohibitive pressure drops are required for practical flow-rate values.

In Table 2, the values of the film mass transfer coefficient, K_f, are presented for different values of the superficial fluid velocity, V_{tp}, in (i) a monolith having skeletons of radius $r_o = 0.75 \cdot 10^{-6}$ m ($d_s = 2r_o = 1.5 \cdot 10^{-6}$ m) and through-pores having diameters of $1.5 \cdot 10^{-6}$–$1.8 \cdot 10^{-6}$ m [14], and (ii) a column packed with spherical particles of radius $r_o = 2.5 \cdot 10^{-6}$ m ($d_p = 2r_o = 5.00 \cdot 10^{-6}$ m). The through-pore diameter range of $1.5 \cdot 10^{-6}$–$1.8 \cdot 10^{-6}$ m in the monolith should be similar [14] to the diameter range of the interstitial channels for bulk flow in the column packed with spherical particles having a diameter of $5.00 \cdot 10^{-6}$ m. The length, L, of the monolith was taken to be the same as the length, L, of the column. The values of the mass transfer coefficient, K_f, were evaluated from Eq. (3) by employing the experimental data reported in Ref. [14]. For a given type of monolith the film mass transfer coefficient, K_f, could be determined from an experiment for a particular value of $\Delta P/L$. This experimental value of K_f will provide the value of the proportionality constant in Eq. (3). Then the values of K_f for different superficial fluid velocities can be obtained from Eq. (3) by inserting in Eq. (3) the measured total pressure drop required by the different superficial fluid velocities. The results in Table 2 indicate that the value of K_f in this monolith [14] is smaller, for a given superficial fluid velocity, V_{tp}, than the value of K_f in the column. This is due to the fact that the total pressure drop, ΔP, in this monolith is smaller [14] than the total pressure drop, ΔP, in the column; for the systems in Table 2, the film mass transfer coefficient, K_f, in the column is about 26% larger than the value of K_f in the monolith. The reasons that make the monolith to require a smaller total pressure drop than the column for the same superficial fluid velocity although the size range of the diameter of the through-pores in the monolith is comparable to the size range of the diameter of the interstitial channels for bulk flow in the bed (the diameter of the interstitial channels is about 1/3 [14] of the diameter, d_p, of the particles, and in this case $d_p = 5.00 \cdot 10^{-6}$ m), are the following: (a) the void fraction in the monolith formed by the through-pores is 0.65 ($\epsilon_{tp} = 0.65$) while the void fraction in the column formed by the interstitial channels for bulk flow is 0.35 ($\epsilon_{tp} = 0.35$), and (b) the through-pores in the monolith are relatively round and straight while the interstitial channels for bulk flow in the column have irregular shape and high tortuosity, because the spherical particles have to be tightly packed [14] in order to produce high efficiency and stability of the packed bed in the column. Of course, the total pressure drop in a column, for a given superficial fluid velocity, can be reduced if particles of larger diameter are employed in the packed bed. The increase in the particle diameter will increase the diffusional intraparticle resistance for mass transfer and this will reduce the efficiency of the separation in the column; it is worth mentioning here that in most systems of liquid chromatography involving packed beds the rate

Table 2
Values of the film mass transfer coefficient, K_f, of BSA for different values of the superficial velocity, V_{tp}, in (i) a monolith having skeletons of diameter $d_s = 2r_o = 1.5 \cdot 10^{-6}$ m and through-pores having diameters of $1.5 \cdot 10^{-6}$–$1.8 \cdot 10^{-6}$ m, and a column packed with spherical particles of diameter $d_p = 2r_o = 5.00 \cdot 10^{-6}$ m

Superficial fluid velocity	Monolith	Column packed with porous particles of radius $r_o = 2.5 \cdot 10^{-6}$ m
V_{tp} (m/s)	K_f (m/s)	K_f (m/s)
$6.944 \cdot 10^{-4}$	$1.482 \cdot 10^{-5}$	$1.867 \cdot 10^{-5}$
$1.388 \cdot 10^{-3}$	$1.864 \cdot 10^{-5}$	$2.352 \cdot 10^{-5}$
$2.777 \cdot 10^{-3}$	$2.351 \cdot 10^{-5}$	$2.962 \cdot 10^{-5}$
$4.165 \cdot 10^{-3}$	$2.691 \cdot 10^{-5}$	$3.392 \cdot 10^{-5}$
$5.554 \cdot 10^{-3}$	$2.962 \cdot 10^{-5}$	$3.731 \cdot 10^{-5}$

controlling mechanism for mass transfer is the diffusion of the molecules of the solute in the pores of the particles.

In Figs. 1–4 simulation results of the breakthrough curves of BSA from a monolith whose skeletons have a radius $r_o = 0.75 \cdot 10^{-6}$ m ($d_s = 2r_o = 1.5 \cdot 10^{-6}$ m) and from columns packed with particles of different radii, are presented. In Figs. 1–4, the solid lines represent the breakthrough curves from the monolith while the broken lines represent the breakthrough curves from the columns packed with spherical particles. The simulation results in Figs. 1–4 were obtained from the numerical solution of Eqs. (1), (4), (6), and (7)–(13). Five different values for the superficial fluid velocity, V_{tp}, were used and the numbers 1, 2, 3, 4 and 5 in Figs. 1–4 indicate the value of the superficial fluid velocity employed in the equations of the mathematical model whose numerical solution provides the results presented in each figure. In Figs. 1–4, the value of V_{tp} for each breakthrough curve is as follows: curve 1: $V_{tp} = 6.944 \cdot 10^{-4}$ m/s (250 cm/h); curve 2: $V_{tp} = 1.388 \cdot 10^{-3}$ m/s (500 cm/h); curve 3: $V_{tp} = 2.777 \cdot 10^{-3}$ m/s (1000 cm/h); curve 4: $V_{tp} = 4.165 \cdot 10^{-3}$ m/s (1500 cm/h); and curve 5: $V_{tp} = 5.554 \cdot 10^{-3}$ m/s (2000 cm/h). The value of the pore diffusion coefficient, D_{mp}, of BSA in the pores of the skeletons of the monolith or in the pores of the spherical particles packed in the column, was taken to be equal to $7.760 \cdot 10^{-12}$ m^2/s for all systems presented in Figs. 1–4. By examining the data in Table 1, one can observe that $7.760 \cdot 10^{-12}$ m^2/s is the highest value of D_{mp} and is obtained from the porous structure of a skeleton or of a particle whose pore size distribution is PSD III and the value of its pore connectivity, n_T, is equal to six. Four different sizes for the radius of the spherical particles in the column were considered and their values are as follows: $r_o = 2.5 \cdot 10^{-6}$ m; $r_o = 5.0 \cdot 10^{-6}$ m; $r_o = 10.0 \cdot 10^{-6}$ m; and $r_o = 15.0 \cdot 10^{-6}$ m. The values of other parameters that were held constant for all simulations are listed in Table 3. The values of $C_{smp,max}$ and K in Table 3 indicate that

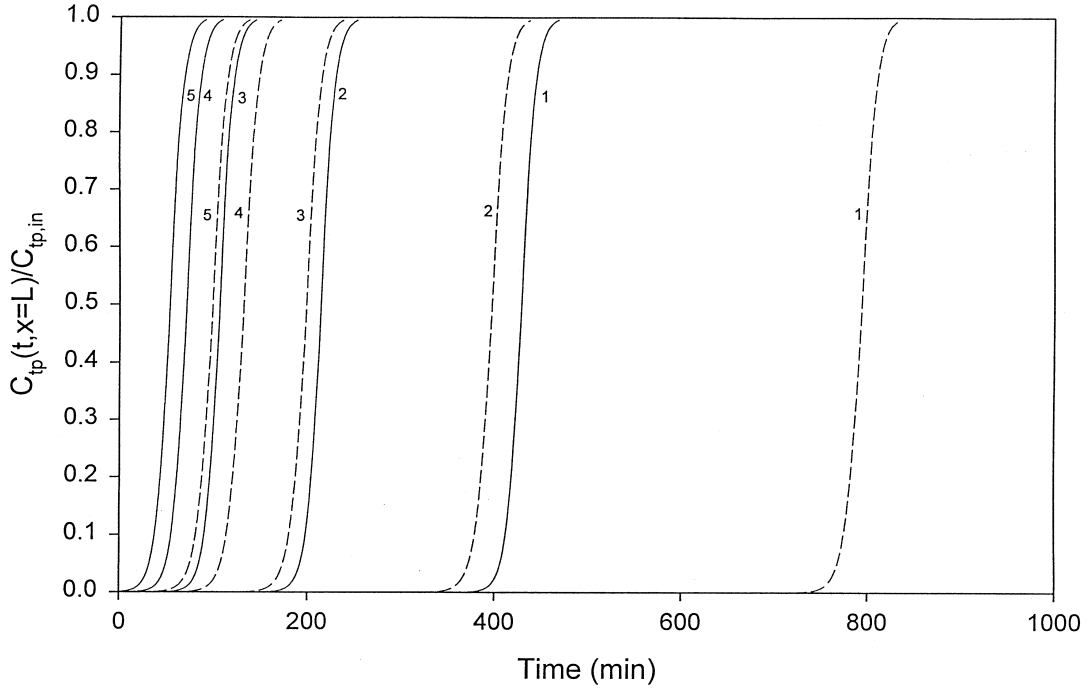

Fig. 1. Breakthrough curves of BSA from monolith (solid lines) and a packed bed (broken lines) of porous spherical particles whose radius, r_o, is $2.5 \cdot 10^{-6}$ m. Curves: 1, $V_{tp} = 6.944 \cdot 10^{-4}$ m/s; 2, $V_{tp} = 1.388 \cdot 10^{-3}$ m/s; 3, $V_{tp} = 2.777 \cdot 10^{-3}$ m/s; 4, $V_{tp} = 4.165 \cdot 10^{-3}$ m/s; and 5, $V_{tp} = 5.554 \cdot 10^{-3}$ m/s.

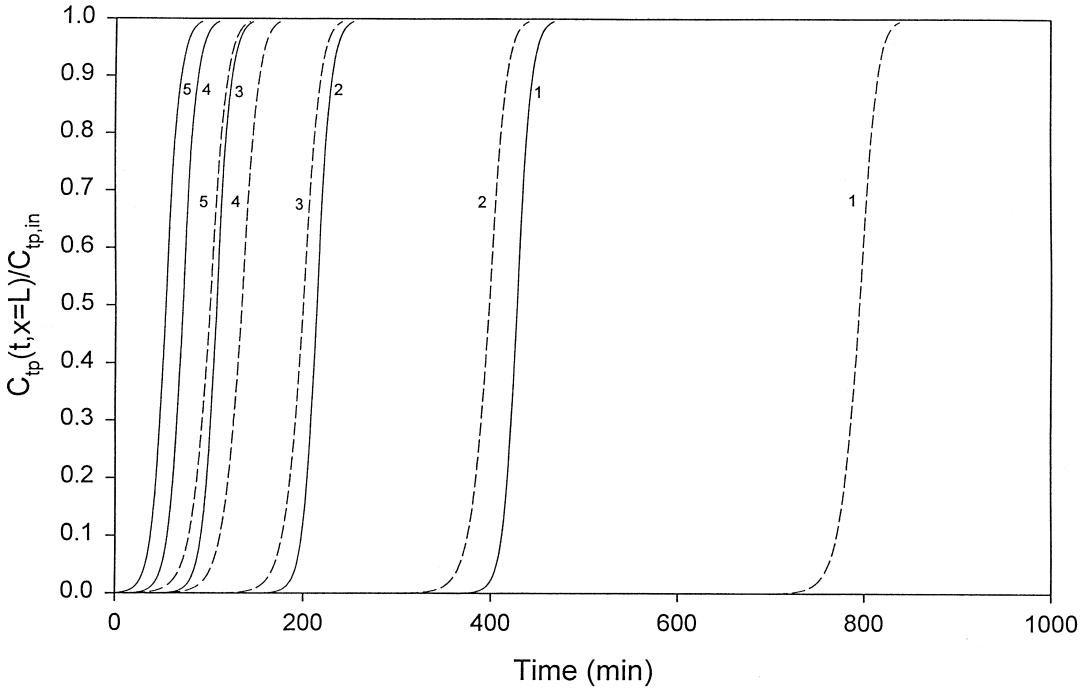

Fig. 2. Breakthrough curves of BSA from monolith (solid lines) and a packed bed (broken lines) of porous spherical particles whose radius, r_o, is $5.0\cdot10^{-6}$ m. Curves: 1, $V_{tp}=6.944\cdot10^{-4}$ m/s; 2, $V_{tp}=1.388\cdot10^{-3}$ m/s; 3, $V_{tp}=2.777\cdot10^{-3}$ m/s; 4, $V_{tp}=4.165\cdot10^{-3}$ m/s; and 5, $V_{tp}=5.554\cdot10^{-3}$ m/s.

the adsorption isotherm is favorable. It is worth noting, as shown in Table 3, that the void fraction in the monolith is 1.857 (0.65/0.35=1.857) times larger than that in the packed bed (column) and this implies that the packed bed contains 1.857 times more adsorbing material. The values of the film mass transfer coefficient, K_f, for the column packed with particles of radius $r_o=2.5\cdot10^{-6}$ m are presented in Table 2. The value of K_f for a given superficial fluid velocity in a column packed with particles whose radius is larger than $2.5\cdot10^{-6}$ m, was obtained from the following expression [52]:

$$K_f|_{V_{tp},r_o>2.5\cdot10^{-6}\,m} = K_f|_{V_{tp},\,r_o=2.5\cdot10^{-6}\,m}\left[\frac{2.5\cdot10^{-6}\,m}{r_o}\right]^{2/3} \quad (15)$$

In the right-hand-side of Eq. (15) the value used for r_o should be greater than $2.5\cdot10^{-6}$ m. It is well established experimentally that as the radius of the particles packed in a column increases, the total pressure drop, for a given superficial fluid velocity, V_{tp}, decreases, and therefore, the film mass transfer coefficient, K_f, of the solute would also decrease as Eq. (3) clearly indicates. Eq. (15) shows that, for a given superficial fluid velocity, V_{tp}, the film mass transfer coefficient, K_f, decreases as the radius of the particles in the packed bed increases. But Eq. (15) provides a correlation that is applicable only to packed beds while Eq. (3) provides an expression for K_f derived from fundamental physical equations [18] and it is applicable to monoliths and to columns packed with particles.

The results in Figs. 1–4 indicate that the breakthrough curves obtained from the monolith are steeper than those obtained from the columns packed with porous spherical particles, especially when the breakthrough curves from the monolith are compared with those obtained from columns packed with particles whose radius, r_o, is greater than or equal to $5.00\cdot10^{-6}$ m. In Fig. 5, the dimensionless dynamic adsorptive capacity $M_{T,ads}/M^*_{T,ads}$ is plotted versus the superficial fluid velocity, V_{tp}, for the monolith and the packed beds at 5% breakthrough. The

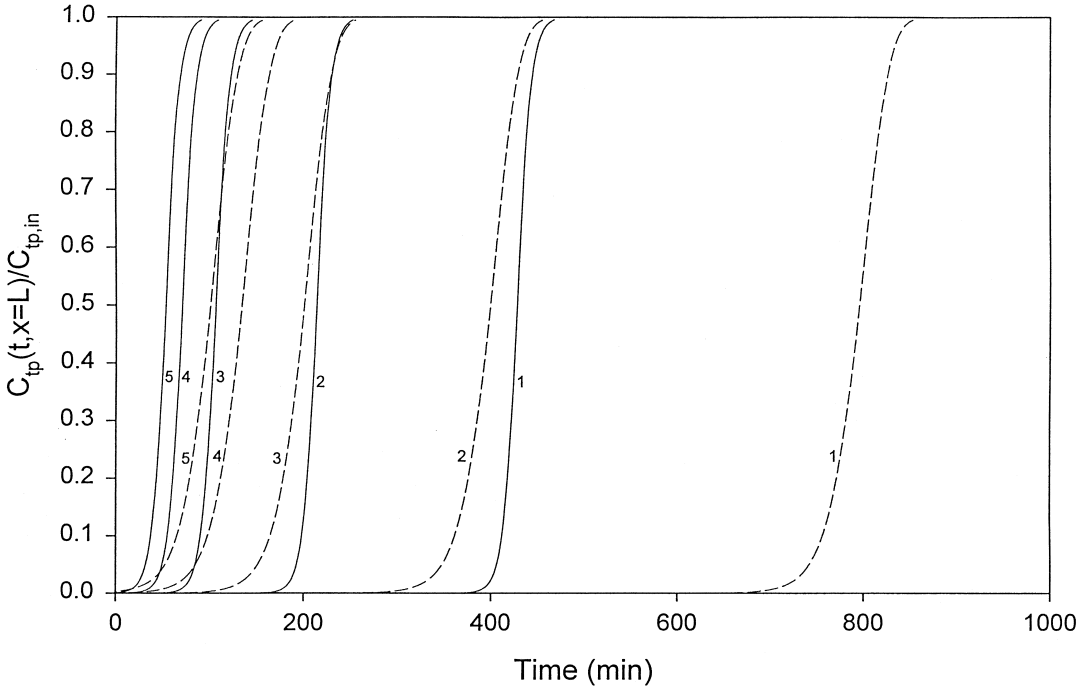

Fig. 3. Breakthrough curves of BSA from monolith (solid lines) and a packed bed (broken lines) of porous spherical particles whose radius, r_o, is $10.0 \cdot 10^{-6}$ m. Curves: 1, $V_{tp} = 6.944 \cdot 10^{-4}$ m/s; 2, $V_{tp} = 1.388 \cdot 10^{-3}$ m/s; 3, $V_{tp} = 2.777 \cdot 10^{-3}$ m/s; 4, $V_{tp} = 4.165 \cdot 10^{-3}$ m/s; and 5, $V_{tp} = 5.554 \cdot 10^{-3}$ m/s.

variable $M_{T,ads}$ represents the total amount of solute (BSA) in the adsorbed phase of the monolith or of the packed bed at 5% breakthrough. The parameter $M^*_{T,ads}$ denotes the total amount of solute (BSA) that could have been in the adsorbed phase of the monolith or of the packed bed if the concentration, C_{smp}, of the solute in the adsorbed phase was in equilibrium with the concentration, $C_{tp,in}$, of the solute in the fluid phase entering the monolith or the packed bed. The value of $M^*_{T,ads}$ for the monolith is $6.826 \cdot 10^{-5}$ kg and for the packed beds is $12.678 \cdot 10^{-5}$ kg. The difference in the values of $M^*_{T,ads}$ for the monolith and the packed beds is due to the fact that the packed beds contain 1.857-times more adsorbing material than the monolith, as discussed above. Fig. 5 clearly shows that the dynamic adsorptive capacity of the monolith is higher than that of the packed beds for all values of the superficial fluid velocity, V_{tp}, as has also been found experimentally [14]. Furthermore, the results in Fig. 5 show that the dynamic adsorptive capacity of the packed beds decreases as the particle radius, r_o, increases.

The value of the pore diffusivity, D_{mp} ($D_{mp} = 7.760 \cdot 10^{-12}$ m^2/s), selected for the comparisons of the dynamic adsorptive capacity between the monolith and the packed beds in Fig. 5, provides the most favorable possible performance for the packed beds. Employing lower values for the pore diffusivity, D_{mp}, from Table 1 will result in even more inferior performance of the packed beds when compared with the performance of the monolith.

4. Conclusions and remarks

A mathematical model was presented that could be used to describe the dynamic behavior, scale-up, and design of monoliths involving the adsorption of a solute of interest. The value of the pore diffusivity of the solute in the pores of the skeletons was determined in an a priori manner by employing the pore network modeling theory of Meyers and Liapis [15,16]. The results clearly show that the pore diffusion coefficient, D_{mp}, of the adsorbate molecules

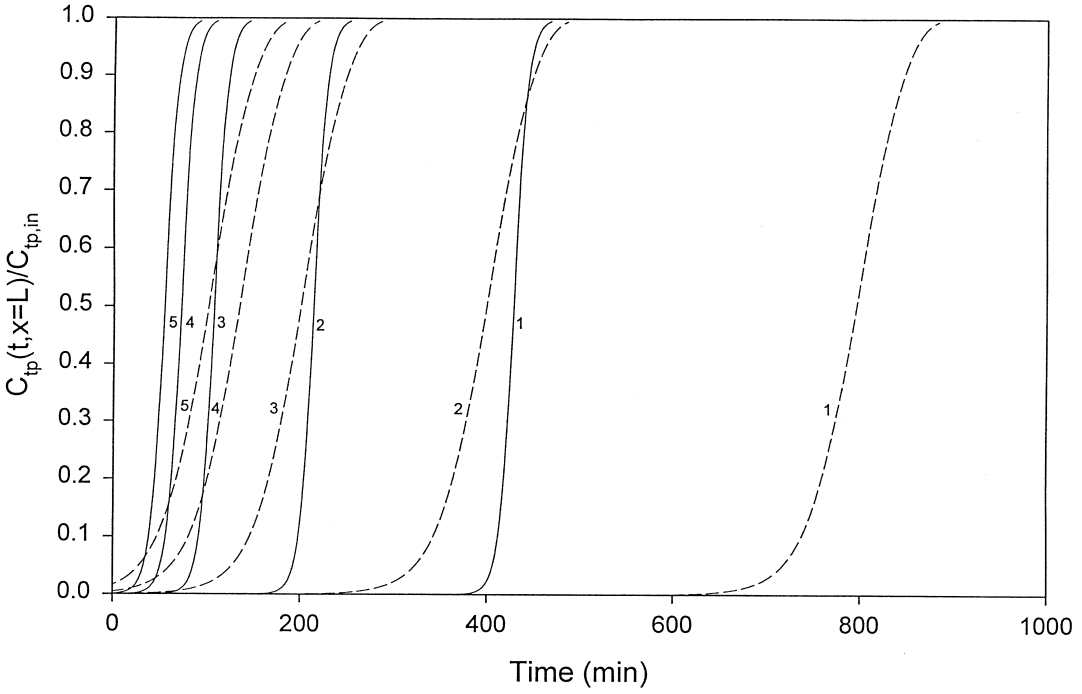

Fig. 4. Breakthrough curves of BSA from monolith (solid lines) and a packed bed (broken lines) of porous spherical particles whose radius, r_o, is $15.0\cdot10^{-6}$ m. Curves: 1, $V_{tp}=6.944\cdot10^{-4}$ m/s; 2, $V_{tp}=1.388\cdot10^{-3}$ m/s; 3, $V_{tp}=2.777\cdot10^{-3}$ m/s; 4, $V_{tp}=4.165\cdot10^{-3}$ m/s; and 5, $V_{tp}=5.554\cdot10^{-3}$ m/s.

Table 3
Values of the parameters and functional form of the pore size distribution of the BSA adsorption system that were held constant in all simulations for both the monolith and the columns packed with spherical particles

Parameter/function	Monolith	Column packed with porous spherical particles
$C_{smp,max}$	50.82 kg/m^3	50.82 kg/m^3
$C_{tp,in}$	0.10 kg/m^3	0.10 kg/m^3
d_p		[$5.00\cdot10^{-6}$–$30.00\cdot10^{-6}$ m]
d_s	$1.50\cdot10^{-6}$ m	
D_{tp}	0	0
D_{mp}	$7.760\cdot10^{-12}$ m^2/s	$7.760\cdot10^{-12}$ m^2/s
k_1	$2.35\cdot10^{-2}$ m^3/(kg s)	$2.35\cdot10^{-2}$ m^3/(kg s)
k_2	$5.17\cdot10^{-6}$ s^{-1}	$5.17\cdot10^{-6}$ s^{-1}
$K=k_1/k_2$	4545.45 m^3/kg	4545.45 m^3/kg
L	0.10 m	0.10 m
n_T	6.00	6.00
Pore size distribution within the skeleton and spherical particle	PSD III	PSD III
R_c	0.0035 m	0.0035 m
ϵ_{mp}	0.60	0.60
ϵ_{tp}	0.65	0.35

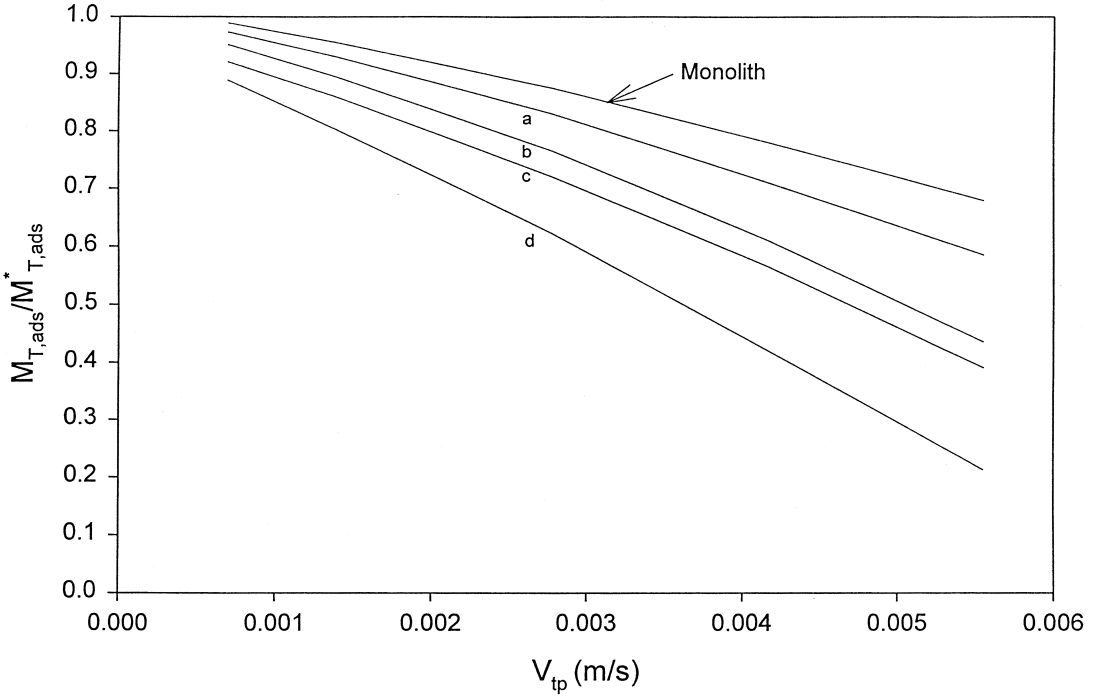

Fig. 5. Dimensionless dynamic adsorptive capacity of monolith and of packed beds for BSA at 5% breakthrough as a function of the superficial fluid velocity, V_{tp}. Curve a: packed bed with spherical particles of radius $r_o = 2.5 \cdot 10^{-6}$ m; curve b: packed bed with spherical particles of radius $r_o = 5.0 \cdot 10^{-6}$ m; curve c: packed bed with spherical particles of radius $r_o = 10.0 \cdot 10^{-6}$ m; and curve d: packed bed with spherical particles of radius $r_o = 15.0 \cdot 10^{-6}$ m.

depends on both the pore size distribution and the pore connectivity, n_T, of the pores in the skeletons. It was shown that, for a given type of monolith, the film mass transfer coefficient, K_f, of the solute in the monolith could be determined from experiments based on Eq. (3) which was derived by Liapis [18] from fundamental physics.

The mathematical model presented in this work was numerically solved in order to study the dynamic behavior of the adsorption of BSA in a monolith having skeletons of radius $r_o = 0.75 \cdot 10^{-6}$ m and through-pores having diameters of $1.5 \cdot 10^{-6}$–$1.8 \cdot 10^{-6}$ m [14]. The breakthrough curves of the BSA obtained from the monolith were steeper than those from columns packed with porous spherical particles whose radii ranged from $2.50 \cdot 10^{-6}$ m to $15.00 \cdot 10^{-6}$ m. Furthermore, and most importantly, the dynamic adsorptive capacity of the monolith was always greater than that of the packed beds for all values of the superficial fluid velocity, V_{tp}.

The results of this work indicate that since in monoliths the size of through-pores could be controlled independently from the size of the skeletons, then if one could construct monolith structures having (a) relatively large through-pores with high through-pore connectivity that can provide high flow-rates at low pressure drops and (b) small-sized skeletons (skeletons having low values of r_o) with mesopores having an appropriate pore size distribution (mesopores having diameters that are relatively large when compared with the diameter of the diffusing solute) and high pore connectivity, n_T, the following positive results, which are necessary for obtaining efficient separations, could be realized: (i) the value of the pore diffusion coefficient, D_{mp}, of the solute would be large, (ii) the diffusion path length in the skeletons would be short, (iii) the diffusion velocity, v_D, would be high, and (iv) the diffusional response time, t_{drt}, would be small. Monoliths with such pore structures could provide more efficient separations with respect to (a) dynamic adsorptive capacity and (b) required pressure

drop for a given flow-rate, than columns packed with porous particles.

5. Notation

C_{mp} concentration of adsorbate in the pore fluid of skeletons or in the pore fluid of particles, kg/m^3

C_{smp} concentration of adsorbate in the adsorbed phase of skeletons or in the adsorbed phase of particles, kg/m^3

$C_{smp,max}$ maximum concentration of adsorbate in the adsorbed phase when all available (accessible) active sites are utilized, kg/m^3

C_{tp} concentration of adsorbate in the flowing fluid phase in the through-pores of the monolith or in the interstitial channels for bulk flow in the packed bed of particles, kg/m^3

$C_{tp,in}$ concentration of adsorbate at $x<0$ when $D_{tp}>0$ or at $x=0$ when $D_{tp}=0$, kg/m^3

D_{mf} free molecular diffusion coefficient of adsorbate, m^2/s

D_{mp} pore diffusion coefficient of adsorbate in the skeletons or in the particles, m^2/s

D_{tp} axial dispersion coefficient of adsorbate in the through-pores of the monolith or in the interstitial channels for bulk flow in the packed bed of particles, m^2/s

d diameter of pore in porous skeleton or porous particle, m

d_p diameter of porous particles in packed bed ($d_p=2r_o$), m

d_s diameter of skeletons in monolith ($d_s=2r_o$), m

K equilibrium adsorption constant ($K=k_1/k_2$), m^3/kg

K_f film mass transfer coefficient of adsorbate, m/s

k_1 rate constant in Eq. (13), m^3/(kg s)

k_2 rate constant in Eq. (13), s^{-1}

L length of monolith or packed bed (column), m

$M_{T,ads}$ total amount of solute in the adsorbed phase of the monolith or of the packed bed at 5% breakthrough, kg

$M^*_{T,ads}$ total amount of solute in the adsorbed phase of the monolith or of the packed bed if the concentration, C_{smp}, of the solute in the adsorbed phase was in equilibrium with the concentration, $C_{tp,in}$, of the solute in the fluid phase entering the monolith or the packed bed, kg

n_T pore connectivity of the porous network (number of pores connected at a node of the porous network), dimensionless

R_c radius of monolith rod or of column, m

r radial distance in skeleton or in particle, m

r_o radius of skeleton or particle, m

Pe Peclet number ($Pe=v_m\kappa/D_{mf}$), dimensionless

Sh Sherwood number ($Sh=K_f\lambda/D_{mf}$), dimensionless

t time, s

t_{drt} diffusional response time ($t_{drt}=r_o^2/D_{mp}$), s

v_D diffusion velocity of adsorbate in the porous medium, m/s

v_m mean velocity of the fluid in the through-pores of the monolith or in the interstitial channels for bulk flow in the packed bed, m/s

V_{tp} superficial fluid velocity, m/s

x axial distance, m

5.1. Greek symbols

α form factor; 1 and 2 for cylinder and sphere, respectively, dimensionless

γ mean diameter of pores in porous skeleton or porous particle, m

δ hindrance parameter of porous medium, dimensionless

ΔP total pressure drop in the monolith or in the packed bed (column), kg/(m s^2)

ϵ_{mp} void fraction in the skeleton or in the particle, dimensionless

ϵ_{tp} void fraction of the monolith or in the packed bed (column), dimensionless

λ linear characteristic dimension of through-pore in a monolith or of interstitial channel for bulk flow in a packed bed of particles, m

μ viscosity of liquid solution, kg/(m s)

σ standard deviation of the diameter of the pores in porous skeleton or porous particle, m

τ average tortuosity in the porous medium, dimensionless

Acknowledgements

The authors gratefully acknowledge partial support of this work by Monsanto and the Biochemical Processing Institute of the University of Missouri-Rolla.

References

[1] S. Hjerten, J.-L. Liao, R. Zhang, J. Chromatogr. 473 (1989) 273.
[2] C. Fujimoto, J. Kino, H. Sawada, J. Chromatogr. A 716 (1995) 107.
[3] F. Svec, J.M.J. Frechet, Anal. Chem. 64 (1992) 820.
[4] S. Hjerten, K. Nakazato, J. Mohammad, D. Eaker, Chromatographia 37 (1993) 287.
[5] Q.C. Wang, F. Svec, J.M.J. Frechet, Anal. Chem. 65 (1993) 2243.
[6] Y.-M. Li, J.-L. Liao, K. Nakazato, J. Mohammad, L. Terenius, S. Hjerten, Anal. Biochem. 223 (1994) 153.
[7] Q.C. Wang, F. Svec, J.M.J. Frechet, J. Chromatogr. A 669 (1994) 230.
[8] J. Matsui, T. Kato, T. Takeuchi, M. Suzuki, K. Yokoyama, E. Tamiya, I. Karube, Anal. Chem. 65 (1993) 2223.
[9] K. Nakanishi, N. Soga, J. Am. Ceram. Soc. 74 (1991) 2518.
[10] K. Nakanishi, N. Soga, J. Non-Cryst. Solids 139 (1992) 1–13.
[11] K. Nakanishi, N. Soga, J. Non-Cryst. Solids 139 (1992) 14–24.
[12] K. Nakanishi, H. Minakuchi, N. Soga, N. Tanaka, J. Sol-Gel Sci. Technol. 8 (1997) 547.
[13] H. Minakuchi, K. Nakanishi, N. Soga, N. Ishizuka, N. Tanaka, Anal. Chem. 68 (1996) 3498.
[14] H. Minakuchi, K. Nakanishi, N. Soga, N. Ishizuka, N. Tanaka, J. Chromatogr. A 762 (1997) 135.
[15] J.J. Meyers, A.I. Liapis, J. Chromatogr. A 827 (1998) 197.
[16] J.J. Meyers, A.I. Liapis, J. Chromatogr. A 852 (1999) 3.
[17] M.A. McCoy, A.I. Liapis, J. Chromatogr. 548 (1991) 25.
[18] A.I. Liapis, Math. Modelling Sci. Comput. 1 (1993) 397.
[19] A.I. Liapis, Y. Xu, O.K. Crosser, A. Tongta, J. Chromatogr. A 702 (1995) 45.
[20] G.A. Heeter, A.I. Liapis, J. Chromatogr. A 711 (1995) 3.
[21] G.A. Heeter, A.I. Liapis, J. Chromatogr. A 734 (1996) 105.
[22] G.A. Heeter, A.I. Liapis, J. Chromatogr. A 743 (1996) 3.
[23] G.A. Heeter, A.I. Liapis, J. Chromatogr. A 760 (1997) 55.
[24] G.A. Heeter, A.I. Liapis, J. Chromatogr. A 776 (1997) 3.
[25] G.A. Heeter, A.I. Liapis, J. Chromatogr. A 796 (1998) 157.
[26] J.H. Harwell, A.I. Liapis, R. Litchfield, D.T. Hanson, Chem. Eng. Sci. 35 (1980) 2287.
[27] T.K. Sherwood, R.L. Pigford, C.R. Wilke, Mass Transfer, McGraw-Hill, New York, 1975.
[28] G. Stephanopoulos, K. Tsiveriotis, Chem. Eng. Sci. 44 (1989) 2031.
[29] B.H. Arve, A.I. Liapis, AIChE J. 33 (1987) 179.
[30] B.H. Arve, A.I. Liapis, Biotechnol. Bioeng. 30 (1987) 638.
[31] B.H. Arve, A.I. Liapis, Biotechnol. Bioeng. 31 (1988) 240.
[32] B.H. Arve, A.I. Liapis, Biotechnol. Bioeng. 32 (1988) 616.
[33] J.H. Petropoulos, A.I. Liapis, N.P. Kolliopoulos, J.K. Petrou, N.K. Kanellopoulos, Bioseparation 1 (1990) 69.
[34] A. Johnston, M.T.W. Hearn, J. Chromatogr. 512 (1990) 101.
[35] A.I. Liapis, H. Sadikoglu, O.K. Crosser, J. Chromatogr. A 828 (1998) 345.
[36] A.I. Liapis, M.A. McCoy, J. Chromatogr. 599 (1992) 87.
[37] M.A. McCoy, A.I. Liapis, K.K. Unger, J. Chromatogr. 644 (1993) 1.
[38] D.D. Frey, E. Schweinheim, C. Horvath, Biotechnol. Prog. 9 (1993) 273.
[39] G. Carta, M.E. Gregory, D.J. Kirwan, H.A. Massaldi, Sep. Technol. 2 (1992) 62.
[40] G. Carta, A.E. Rodrigues, Chem. Eng. Sci. 48 (1993) 3927.
[41] A.I. Liapis, M.A. McCoy, J. Chromatogr. A 660 (1994) 85.
[42] Y. Xu, A.I. Liapis, J. Chromatogr. A 724 (1996) 13.
[43] J. Villadsen, M.L. Michelsen, Solution of Differential Equation Models by Polynomial Approximation, Prentice-Hall, Englewood Cliffs, NJ, 1978.
[44] C.D. Holland, A.I. Liapis, Computer Methods for Solving Dynamic Separation Problems, McGraw-Hill, New York, 1983.
[45] T. Wicks, Scientific Computing and Analysis Library Report, SCA-LR-52, Boeing Computer Services, Seattle, WA, 1988.
[46] J.K. Petrou, J.H. Petropoulos, N.K. Kanellopoulos, A.I. Liapis, in: A.B. Mersmann, S.E. Scholl (Eds.), Proceedings of the 3rd International Conference on Fundamentals of Adsorption, Engineering Foundation, New York, 1990, p. 679.
[47] J.H. Petropoulos, J.K. Petrou, A.I. Liapis, Ind. Eng. Chem. Res. 30 (1991) 1281.
[48] H.A. Sober (Ed.), Handbook of Biochemistry – Selected Data for Molecular Biology, The Chemical Rubber Company, Cleveland, OH, 1968.
[49] H. Brenner, L.J. Gaydos, J. Colloid Interface Sci. 58 (1977) 312.
[50] A.I. Liapis, Sep. Purif. Methods 19 (1990) 133.
[51] N.W. Carlson, J.S. Dranoff, in: A.I. Liapis (Ed.), Proceedings of the 2nd International Conference on Fundamentals of Adsorption, Engineering Foundation, New York, 1987, p. 129.
[52] C.J. Geankoplis, Transport Processes and Unit Operations, Prentice Hall, Englewood Cliffs, NJ, 1993.